Polymer Bulletin (2026) 83:203
https://doi.org/10.1007/s00289-025-06242-z

ORIGINAL PAPER

Nanocellulose/Graphene oxide-modified PVDF membranes for efficient dye removal from wastewater: synthesis, characterization, and performance evaluation

Md. Rezaur Rahman[1] · Nur Fatmadewi Dollah Chek[1] · Muhammad Khusairy Bin Bakri[1,2] · M. Shahabuddin Ahmmad[3] · Muneera S. M. Al-Saleem[4] · Jehan Y. Al-Humaidi[4] · Mohammed M. Rahman[5]

Received: 4 July 2025 / Revised: 18 October 2025 / Accepted: 14 December 2025

Abstract

Water pollution has remained a pressing global concern, particularly as access to clean water becomes increasingly limited. Wastewater treatment plays a crucial role in ensuring sufficient water can be supplied for daily needs. Membrane technology has become a promising method in ensuring the efficiency of eliminating contaminants from the wastewater, whereby poly(vinylidene fluoride) (PVDF) is commonly used in membrane fabrication. However, PVDF often faces limitations related to fouling, hydrophobicity, and mechanical stability, which can affect its long-term performance. To overcome these limitations, this research aims to develop, characterize, and analyze the performance of PVDF/GO/NC membranes for dye removal. The membranes were developed using the NIPS method, and characterization to determine the physical and chemical properties of the developed membranes was conducted using Fourier transform infrared (FTIR) spectroscopy, Scanning Electron Microscopy (SEM), X-ray diffraction (XRD), membrane porosity measurement, and Ultraviolet-visible (UV-vis) spectroscopy. The membrane performance was evaluated through water permeation flux and dye removal efficiency using methylene blue (MB) as a model dye. The incorporation of nanocellulose (NC) and graphene oxide (GO) is expected to enhance the hydrophilicity, antifouling properties, and overall filtration performance of PVDF membranes, offering a more sustainable and effective approach to wastewater treatment.

Keywords Poly(vinylidene fluoride) (PVDF) · Nanocellulose (NC) · Graphene oxide (GO) · Membrane technology · Wastewater treatment

Extended author information available on the last page of the article

Published online: 09 January 2026

Introduction

Water is a vital life ingredient that is employed as a nutrient carrier medium and to maintain health. Potable water is required for the absence of disease and the maintenance of ecosystems. However, according to the United Nations [23], 2.2 billion people lack access to safe drinking water, and 4.2 billion people lack adequate sanitation, with nearly 80% of wastewater discharged untreated. Increasing demand and limited availability of freshwater necessitate wastewater treatment. Wastewater contains a range of contaminants like heavy metals, pharmaceuticals, pathogens, endocrine disruptors, nutrients, and dyes [22].

Among these, dye effluents pose serious environmental issues due to their toxicity, complex nature, and resistance to biodegradation. Nearly 800,000 tons of dyes are produced annually, and 10–15% of them are released into the wastewater with a concentration of up to 300 mg/L, posing threats to aquatic life [9]. Textile wastewater may contain toxic heavy metals such as mercury, chromium, cadmium, lead, and arsenic [3]. Left untreated, dyes alter water clarity, reduce light penetration and inhibit photosynthesis, reduce dissolved oxygen, and interfere with aquatic food chains [18, 20]. Conventional processes such as flocculation and electrodialysis remain ineffective for dye removal [9].

Membrane technology has been recognized as a possible option due to its high efficiency of pollutant removal, low area requirements, and stability of operation [24]. Polyvinylidene fluoride (PVDF) is one of the most used fabric materials for membranes due to mechanical resistance, thermal stability, and processability [15]. Nevertheless, its hydrophobic nature is responsible for fouling, which decreases efficiency and lifespan [7, 19]. Incorporation of nanomaterials has been investigated to enhance hydrophilicity and antifouling properties.

Nanocellulose (NC), derived from renewable cellulose, offers high surface area, mechanical properties, and hydrophilicity, and increases polymer composite performance even at low loadings [8]. Graphene oxide (GO), with its high surface area and oxygenated functional groups, is highly adsorbent, hydrophilic, and has tunable transport channels for eliminating contaminants [4, 5]. This study prepares PVDF membranes with NC and GO to amplify porosity, hydrophilicity, antifouling resistance, and dye removal efficiency.

Methodology

Materials and reagents

The NC powder used in this research was obtained from the *Gigantochloa scortechinii* species. Poly(vinylidene fluoride) (PVDF) (Cas no. 24937-79−9, molecular weight: 534 000 g mol^{-1}), graphene oxide (GO) (paste, non-exfoliated) (900704–100 g) and silver nitrate ($AgNO_3$) (Index-No.: 047-00100–2) were obtained from Sigma Aldrich Sdn (Petaling Jaya, Malaysia) while dimethylacetamide (DMAc) (CAS no. 127-19−5, molecular weight: 87.12) was obtained from Thermo Fisher

Table 1 Compositions of dope solution in wt%

Membrane sample	PVDF (wt%)	DMAc (wt%)	$AgNO_3$ (wt%)	GO (wt%)	NC (wt%)
S0 – PVDF	8.67	81.51	5.78	0.00	0.00
S1 – PVDF/NC	8.67	81.51	5.78	0.00	1.48
S2 – PVDF/GO/NC	8.67	81.51	5.78	2.89	1.16
S3 – PVDF/GO/NC	8.67	81.51	5.78	5.63	0.84
S4 – PVDF/GO/NC	8.67	81.51	5.78	8.24	0.55
S5 – PVDF/GO/NC	8.67	81.51	5.78	10.72	0.27
S6 – PVDF/GO	8.67	81.51	5.78	1.45	0.00

Table 2 Compositions of dope solution in grams (g) and milliliters (ml)

Membrane sample	PVDF (g)	DMAc (ml)	$AgNO_3$ (g)	GO (ml)	NC (g)
S0 – PVDF	6.0	60.0	0.40	0.0	0.0
S1 – PVDF/NC	6.0	60.0	0.40	0.0	1.00
S2 – PVDF/GO/NC	6.0	60.0	0.40	2.0	0.80
S3 – PVDF/GO/NC	6.0	60.0	0.40	4.0	0.60
S4 – PVDF/GO/NC	6.0	60.0	0.40	6.0	0.40
S5 – PVDF/GO/NC	6.0	60.0	0.40	8.0	0.20
S6 – PVDF/GO	6.0	60.0	0.40	1.0	0.00

Scientific (Shah Alam, Selangor). The ultrapure water and deionized water used in this research were supplied by Universiti Malaysia Sarawak (UNIMAS).

Preparation of nanocomposite membranes

Preparation of pristine Membrane, PVDF/NC, PVDF/GO/NC, and PVDF/GO dope solution

GO dispersion was initially prepared by dissolving 3.00 g of GO paste into 60.0 ml DMAc at a temperature of 70°C for 90 min and continuously stirred for 24 h. Then the dispersion was placed in the sonicator for 60 min and centrifuged for 15 min. The nanocomposite membranes were prepared using the NIPS method, which was adapted from [16]. For the pristine membrane (S0), 8.67 wt% PVDF and 5.78 wt% $AgNO_3$ were dissolved into 81.51 wt% DMAc at a temperature of 70°C for 90 min and continuously stirred until all of the materials were completely dissolved in the solvent and a homogenous solution was obtained. The solution obtained was known as a dope solution. The dope solution was continuously stirred for 24 h at a constant temperature of 50°C and 300 rpm. A similar procedure was conducted for Sample 1 (S1) to Sample 5 (S5) by varying the volume and weight of GO and NC, respectively. Sample 6 (S6) was prepared by using the same procedure as S0 by substituting NC with 1.45 wt% GO dispersion. The different composition of the material of each membrane sample was prepared as shown in Tables 1 and 2.

Casting of nanocomposite membrane

Two coagulation baths that contained deionized (DI) water were prepared and labeled, where the first coagulation bath was for the first immersion upon casting, with a maximum of 20 min of immersion, and the second coagulation bath was for the immersion of the casted membrane from the first coagulation bath, which was further immersed for 24 h. Once the dope solution was prepared overnight, the casting process was conducted by pouring approximately 30 ml of the dope solution onto a smooth glass panel with a dimension of 22 cm × 30 cm. A glass rod was then used to roll the solution onto the glass panel. The glass rod was rolled with constant pressure to ensure consistency in the thickness of the membrane. The casted membrane was then immersed in the first coagulation bath for a maximum of 20 min to ensure the residual solvent and non-solvent additives from the casting process were eliminated. Then, the casted membrane from the first coagulation bath was transferred into the second coagulation bath and immersed for 24 h. After 24 h, the membranes were kept immersed in a container with ultrapure water and placed in the refrigerator at 5°C until further characterization was conducted. Pebbles, which act as the weight, were placed on the membrane sheets to prevent the membranes from floating and ensure it completely immersed in the water.

Drying of nanocomposite membrane

After seven days, the wet membranes were placed on aluminum sheets and left to dry (air-dry) for three days. Once the membranes dried, they were placed inside the zip-lock bags and labeled accordingly. The bags were placed in the desiccator upon further characterization. A few sheets of membranes were left immersed in the ultrapure water in their respective containers and were kept refrigerated for the performance evaluation test.

Characterization of nanocomposite membrane

Fourier transform infrared (FTIR) spectroscopy analysis

FTIR 'IR Affinity-1' spectroscopy (Shimadzu) was used to identify functional groups and characterise molecular bonds through the observation of IR spectrum bands at a range of 4000 to 400 cm-1. The membrane sample (1 cm x 1 cm) was cut and placed onto the holder known as the ATR-FTIR crystal. Then, the swivel press was used to press down the sample and crystal.

Scanning electron microscopy (SEM) analysis

A JEOL JSM-639OLA Analytical was used to observe the morphological images of the membrane samples. The sample was mounted on aluminum stubs and coated using 'JFC-1600' (JEOL (Japan) Ltd). Images of the sample surface were captured using a field emission gun with a voltage of 10 kV.

X-ray diffraction (XRD) analysis

X-ray diffraction (XRD) analysis was performed to assess the crystallinity of the samples and identify crystalline phases. The membrane samples were examined at room temperature using a Rigaku SmartLab Powder X-ray diffractometer with CuKα radiation (λ = 1.5418 Å). The XRD patterns were recorded over a scattering angle (2θ) range of 5° to 90° at a scanning rate of 2° min^{-1}.

Membrane porosity measurement

The membrane porosity (ε) was determined using the gravimetric method in Eq. (1).

$$\epsilon\ \% = \frac{\left(\frac{W_{wm}-W_{dm}}{\rho_{water}}\right)}{\left(\frac{W_{wm}-W_{dm}}{\rho_{water}}\right)+\left(\frac{W_{dm}}{\rho_{PVDF}}\right)} \times 100 \quad (1)$$

where, W_{wm}: weight of wet membrane (g), W_{dm}: weight of dry membrane (g), ρ_{water}: density of water (0.998 g cm^{-3}), and ρ_{PVDF}: density of PVDF polymer (1.740 g cm^{-3}).

Ultraviolet-visible (UV-vis) spectroscopy for dye removal concentration analysis

A UV-160 UV-Vis-NIR spectrophotometer (Shimadzu Scientific Instruments, Inc., Tokyo, Japan) was used to determine the concentration of dye before and after the dye removal test. 5 mL of the sample was transferred into a UV-Vis cuvette and analyzed using a UV-vis spectrophotometer. The wavelength range for the MB dye solution was set between 500 and 700 nm. A calibration curve was established using reference solutions with known concentrations of 2.0, 4.0, and 6.0 ppm of MB.

Membranes performance evaluation

Water permeation flux

Flat sheet nanocomposite membrane samples, each with a diameter of 4.4 cm, were cut and placed in the membrane holder of the cross-flow water filtration system. The membranes were secured using a rubber O-ring, which ensured proper positioning within the holder. The system featured an effective membrane filtration area of 1.52×10^{-3} m^2. Before testing, the membranes underwent a 30-minute pre-compression at 2 bar pressure to stabilize the flux. Following this, the pressure was reduced to 1 bar, and the permeate volume was recorded every 10 min over 70 min. The applied pressure acted as the driving force for water permeation through the membrane. The water permeation flux was determined by calculating the ratio of permeate volume to permeation time, as described in Eq. (2). Each membrane sample underwent three permeation flux tests to determine the average value and standard deviation.

$$J_w = \frac{V}{A \times \Delta T} \quad (2)$$

where, J_W: water permeation flux (L/m^2.h), V: permeate volume (m^3), A: effective area of membrane (m^2), and ΔT: filtration time (h).

Dye removal

A 2 ppm MB dye solution was prepared to be used as the feed for the membrane removal test. The initial dye concentration was verified using a UV-160 UV-Vis-NIR spectrophotometer (Shimadzu Scientific Instruments, Inc., Tokyo, Japan) at a wavelength of 664 nm, which corresponds to the maximum absorbance of MB. Before testing, the membranes underwent a 30-minute pre-compression at 2 bar pressure to stabilize the flux. After ensuring that the system had stabilized, 1000 mL of 2 ppm MB dye solution was poured into the solution tank, and the applied pressure was set to 1 bar at room temperature. The permeate (J_{MB}) was collected, and its volume was recorded every 10 min over 70 min. The dye removal ratio (R) was calculated using Eq. (3). Each membrane sample underwent three dye removal tests to determine the average value and standard deviation.

$$\% \, R = \left(1 - \frac{C_f}{C_i}\right) \times \ 100 \tag{3}$$

where R: dye removal ratio (%), C_f: final MB dye concentration (mg L^{-1}), C_i: initial MB dye concentration (mg L^{-1}).

Results and discussion

Fourier transform infrared (FTIR) spectroscopy analysis

Figure 1(a) shows the FTIR spectra for pristine PVDF (S0). The peaks detected at 879.54 cm^{-1} and 1172.72 cm^{-1}indicated the stretching vibrations of C-C and C-F functional groups, respectively. PVDF is a fluorinated polymer, and the presence of C-F stretching vibrations confirmed the PVDF's fluorinated structures. These peaks are similar to the study by [16], whereby both peaks were presented at 875.68 cm^{-1} and 1174.65 cm$^{-1,}$respectively. [2] also showed stretching vibration of C-F at 1175 cm^{-1}. The C-F functional group in PVDF plays an important role in providing more flexibility, less density, and slight wettability of the polymer [12]. Additionally, the peak at 1400.32 cm^{-1} indicates C-H bending vibrations in the PVDF polymer, which further supports the structural integrity of PVDF. Figure 2 shows the comparison of FTIR spectra for S0-S6, where consistency in the peaks can be observed at 837.11 cm^{-1} to 1400.32 cm$^{-1,}$ indicating the successful incorporation of PVDF as the primary polymer matrix. The 837.11 cm^{-1}peak corresponds to the β-phase of PVDF, confirming its semi-crystalline structure. This has also been confirmed by [6], who mentioned that the range of peaks at 837–841 and 508–512 cm^{-1} has stronger absorbance of β- and γ-phase compared to α-phase. This also indicates the advantage of PVDF as a piezoelectric material, as the β- and γ-phases displayed a piezoelectric effect, which is the ability to generate an electric charge. The 1400.32 cm^{-1}

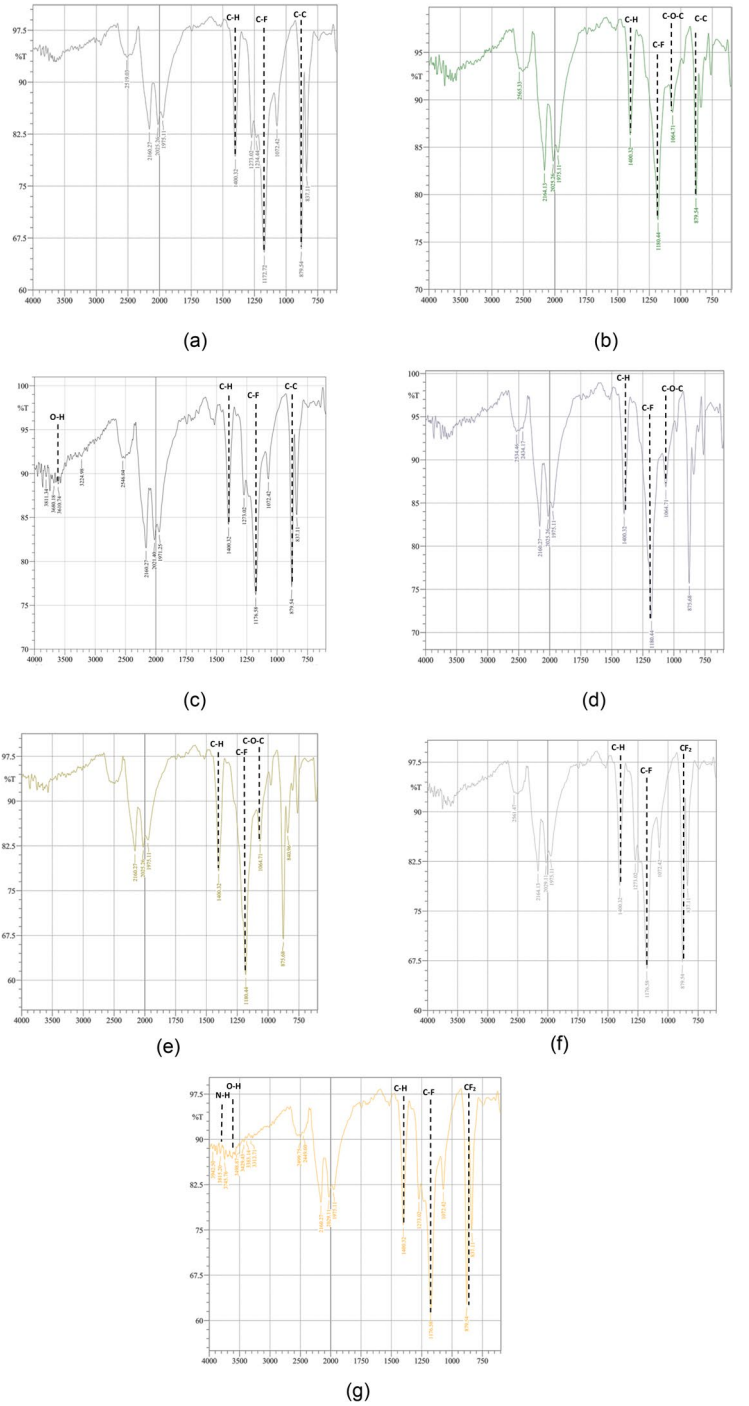

Fig. 1 FTIR spectra for (**a**) PVDF, (**b**) PVDF/NC, (**c**) PVDF/GO, and (**d**) - (**g**) PVDF/NC/GO with varying NC and GO loading

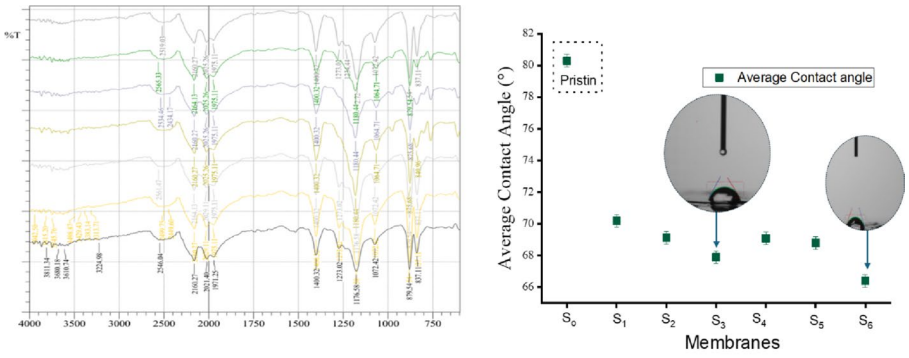

Fig. 2 **(a)** Comparison of FTIR spectra and (**2b**) Water contact angle analysis of S0:PVDF, S1:PVDF/NC, S2-S5:PVDF/NC/GO (with varying NC and GO loading), and S6:PVDF/GO

peak represents C-H bending vibrations inherent to PVDF. The retention of these peaks across all samples suggests that the structural integrity of PVDF remains intact despite modifications.

Additionally, this also confirmed the uniform dispersion of PVDF throughout the membranes. The technique used in membrane fabrication played an important role in ensuring that the materials were uniformly dispersed throughout the solution before the casting process was conducted. Proper dispersion is essential for achieving consistent membrane morphology and performance, as uneven distribution may lead to defects such as phase separation, irregular pore formation, or reduced mechanical integrity. The presence of consistent peaks across all samples further supports the successful incorporation of PVDF, reinforcing its structural uniformity within the membranes.

Upon the addition of NC, the C-O-C stretching vibration is observed at 1064.71 cm^{-1}, which is shown in Fig. 1(b), (d), and (e), where the composition of nanocellulose was 1.48 wt%, 1.16 wt%, and 0.84 wt%, respectively. O-H (hydroxyl) stretching vibrations at 3610.74 cm^{-1} and 3383.14 cm^{-1} are observed in Fig. 1(c) and (g), respectively, indicating the hydrophilicity of the membrane through the addition of GO with 1.45 wt% and 10.72 wt% concentration. These hydrophilic behavior was further validated via contact angle analysis (see Fig. 2b), the results shows a progressively decreased water contact angle with membrane modification which corroborate the influence of nanoparticle in the materials as reported in [10, 13, 25]. The peak detected in Fig.1(c) is similar to [17], where the O-H group for GO/Ag was detected at 3616 cm^{-1}. The presence of O-H indicated the hydrophilicity properties of the membranes, and this is important in improving the antifouling performance of the membrane. A membrane with a hydrophilic surface can perform a hydration layer that can act as a barrier to foulants, thereby enhancing membrane longevity and performance. As reported by [11], membranes with a higher affinity for water make it energetically less favorable for proteins and other biofouling to adhere, thereby improving fouling resistance. A prominent peak at 3429.43 cm^{-1} for S5 is observed, indicating the presence of the stretching vibrations of N-H. This showed that the

silver nitrate was successfully incorporated into the membrane, as the additives are important during the pore formation process.

Scanning electron microscopy (SEM) analysis

SEM analysis is mainly used to analyze the surface cross-section morphologies of the membranes. Figure 3 shows the photographs of dried membranes and SEM analysis for S0 to S6 and detailed insights into the surface morphology of the membranes through SEM images at x5,000 and x10,000 magnifications. S0 indicates pristine membrane; S1-S5 indicates PVDF membranes with varying loadings of NC and GO; and S6 indicates PVDF with GO incorporation only (without NC). From S0 to S6, it is shown that the pores are more prominent as NC and GO were added compared to the pristine membrane (S0). A smooth and uniform surface can be seen on the S0 membrane, where the color appeared whitish upon drying, which is mainly due to the white-colored powder of PVDF during the preparation of the dope solution. The smoothness of the surface cross-section of the membrane is due to low pore formation on the surface, which can be observed in the SEM analysis, where hardly any pores can be seen in the images. The type of solvent used during the phase inversion technique, which in this case, the ultrapure water, affected the surface formation of the membrane. According to [21], using water as the coagulation bath resulted in the formation of an asymmetric membrane structure with a dense skin layer and a porous support layer. The smooth surface and less pore formation played a crucial role in the performance of the membrane, which is discussed in the later section.

Upon the incorporation of 1.48 wt% of NC in S1, the surface of the dried membrane has a rougher texture, and unlike S0, the color appeared greyish. The rough texture on the surface was due to the increased porosity, which can be seen in the SEM images. S2 to S5 exhibited a similar color to S1 when dried and significantly increased surface roughness and pore formation. When NC and GO were added, this promoted the formation of more surface pores, attributed to their hydrophilic nature (refer to Fig. 2b), which enhances phase separation during the phase inversion process. Specifically, the hydroxyl groups in NC and the oxygen-containing functional groups (such as hydroxyl, epoxy, and carboxyl) in GO increase the affinity of these fillers toward the nonsolvent (water) during phase inversion. This accelerates the solvent–nonsolvent exchange rate, leading to faster phase separation and the development of a more porous surface structure. The increased hydrophilicity also lowers the interfacial energy barrier between the polymer solution and the nonsolvent, further promoting nucleation of pores at the membrane surface. This improved porosity is beneficial for membrane permeability, as it facilitates water flux and enhances filtration performance. A membrane with hydrophilicity properties helps to protect the membrane from fouling, as the hydration layer formed on the surface of the membrane can protect the membrane from foulants, which also improves the antifouling performance of the membrane. Undissolved GO can be observed on the surface of S3 and S5 when GO was at 5.63 wt% and 10.72 wt%, respectively, which may have happened due to the non-uniform dispersion in the dope solution as the concentration of GO was increased. Similar results were obtained by [2], where undissolved aminated GO were observed on their membranes as well.

Membrane	Dried membrane	Surface morphology (x 5,000 magnification)	Surface morphology (x 10,000 magnification)
S0 – PVDF	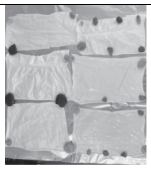	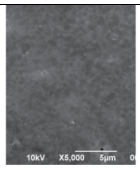	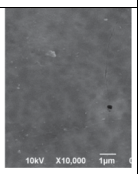
S1 – PVDF/NC	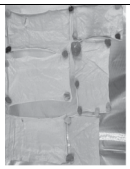	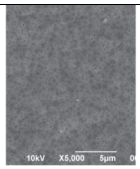	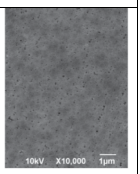
S2 – PVDF/NC/GO		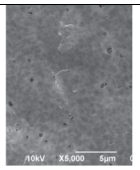	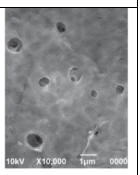
S3 – PVDF/NC/GO		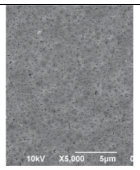	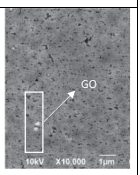
S4 – PVDF/NC/GO		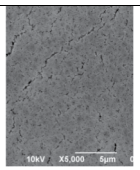	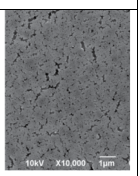
S5 – PVDF/NC/GO		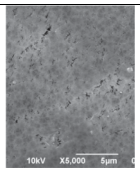	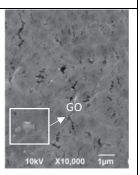
S6 PVDF/GO		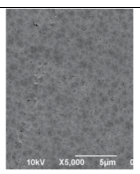	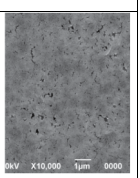

Fig. 3 Photographs of dried membranes and SEM analysis results of the cross-section surface of the nanocomposite membranes

When 2.89 wt% GO was incorporated, fewer and larger pores were seen on the SEM images of S2. Based on Fig. 3, for S3 to S5, surface cracks were observed, which may be due to the agglomeration of fillers at higher concentrations. From S3 to S5, the concentration of NC decreases from 0.84 wt% to 0.27 wt% while GO increases from 5.63 wt% to 10.72 wt%. The increase in the concentration of GO may lead to poor dispersion within the polymer matrix, creating weak points and stress concentrations, resulting in cracking during membrane drying. These cracks can also happen due to unintended stress during the membrane fabrication [16]. The formation of cracks may affect the performance of the membrane negatively, especially on its selectivity, as they could potentially allow undesired pollutants or solutes to pass through. Similarly, S6 also displayed fewer surface pores with some surface cracks. In this case, the absence of NC may have contributed to reduced structural support within the membrane matrix.

Overall, comparing the membranes from S1 to S6, S2 has the largest pores while S0 has the fewest pores. Although S1 has small pore sizes like S3 to S5, the pores are well-dispersed, and no cracks are observed. Due to the absence of NC, S6 exhibited fewer pores on its surface. This indicates that the addition and concentration of added NC and GO have significant impacts on the pore formations and consistencies of the pores, which also affect the porosity and membrane performances in water permeation and dye removal.

X-ray diffraction (XRD) analysis

The XRD patterns for all membrane samples (S0 to S6) are presented in Fig. 4. Amorphous peaks can be observed at around $2\theta = 18.0°$ and $2\theta = 20.0°$, and a prominent crystalline peak at $2\theta = 28.0°$ corresponding to the α-phase crystalline structure of PVDF. The peaks formed were similar to [16], where the peaks were observed approximately at $2\theta = 20.0°$ and $2\theta = 25.0°$. These peaks were present in all samples, indicating that the semi-crystalline nature of PVDF was retained even after modifications with NC and GO with varying loadings. Notably, the intensity of diffraction peaks showed an increase from S0 to S6, with S6 showing the highest peak intensity at approximately 40,000 a.u, indicating a higher degree of crystallinity compared to other samples. This suggests that the addition of 1.45 wt% GO (without NC) influenced the crystalline arrangement of the membrane matrix.

The pristine PVDF membrane (S0) exhibited characteristic peaks of the α-phase, consistent with literature reports on pristine PVDF. The incorporation of NC (S1–S3) slightly increased the crystallinity of the membranes, as evidenced by the sharper and more intense peaks, particularly around $2\theta = 38.0°$. Similar findings were obtained by [16], whereby the incorporation of NC resulted in the presence of β-phase in the XRD result. As the concentration of NC decreased and GO increased, the peaks were not available in S4 and S5, which indicates the reciprocal interaction between NC and GO as the NC blends into the GO structures [14].

The addition of more concentration of GO in S4 to S6 may have caused the intense semi-crystalline peaks, which can be seen at $2\theta = 48.0°$. GO contains functional oxygenated groups that can interact with the PVDF chains via hydrogen bonding, facilitating more ordered polymer chain alignment. This interaction likely explains the

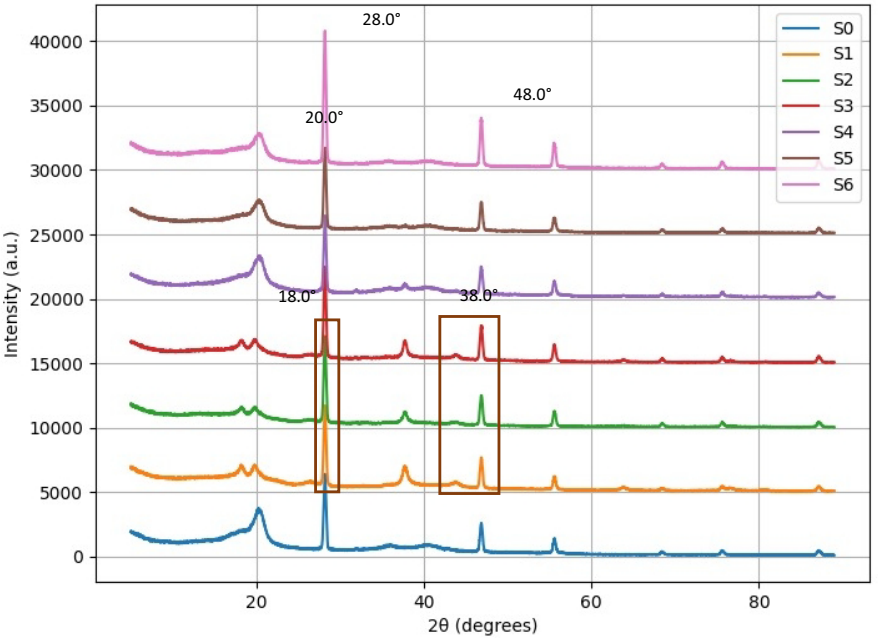

Fig. 4 Comparison of XRD analysis of each membrane sample

significant peak intensities seen in S5 and S6. This can be proven from the FTIR result, where the presence of O-H (hydroxyl) stretching vibrations was detected at 3610.74 cm^{-1} and 3383.14 cm^{-1}. S6 demonstrated the highest crystallinity, possibly due to the addition of GO at optimal loading. The relatively dense structure observed in SEM images is attributed not only to the high crystallinity but also to the combined effects of polymer chain packing and phase inversion conditions during fabrication.

XRD analysis confirmed that the addition of NC and GO to PVDF membranes influences their crystalline behavior. The synergistic interaction between PVDF, NC, and GO enhances the crystalline ordering, with S6 showing the highest intensity peaks. This structural modification may positively impact membrane performance, including dye rejection, mechanical stability, and water permeability.

Membrane porosity measurement

According to [1], membrane porosity is known as the membrane's void volume fraction, whereby a high permeation flux can be obtained with high porosity, indicating that the porosity of the membrane highly affects its permeability. Figure 5 illustrates the porosity values of the membrane samples ranging from 47.93% to 48.54%. The pristine PVDF (S0) exhibited a porosity of 47.93%.

A slight increase was observed in S1 (48.05%) upon the addition of NC (1.48 wt%), suggesting that nanocellulose promotes pore formation. The hydroxyl groups on NC act as hydrophilic sites, which interact with the nonsolvent (water) during the phase inversion process, accelerating solvent–nonsolvent exchange and nucleating

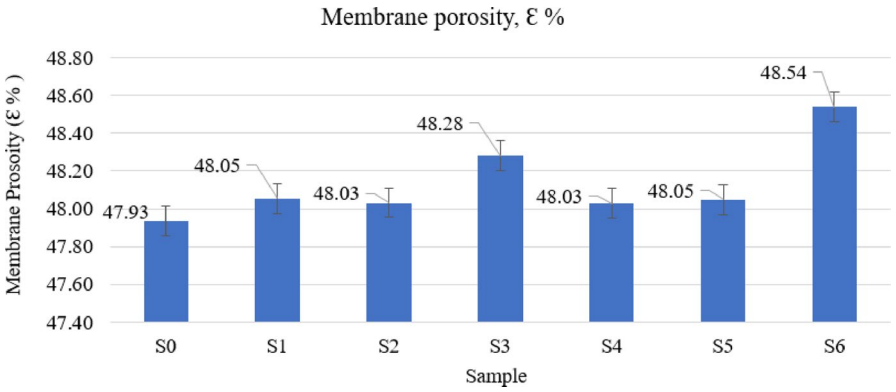

Fig. 5 Membrane porosity of each membrane sample

more pores at the membrane surface and within the matrix. In S2 (NC 1.16 wt%, GO 2.89 wt%), a minor decrease in porosity (48.03%) was observed, which may be attributed to particle agglomeration or increased solution viscosity that hindered phase separation efficiency, causing partial pore collapse.

The porosity recovered in S3 (48.28%) and reached a maximum in S6 (48.54%), likely due to improved dispersion of nanofillers and GO at optimal loadings. The oxygenated functional groups in GO and the hydrophilic NC facilitate uniform nucleation and growth of pores, while silver nanoparticles may act as physical pore formers by locally disrupting polymer chain packing during solvent exchange.

The overall porosity values in this study are relatively lower compared to [2] and [16], where over 70% porosity was achieved. This difference can be attributed to the higher PVDF concentration used in those studies (15–18 wt%), which promotes more open pore formation during phase inversion, whereas our lower polymer concentration favors a denser polymer matrix with smaller voids. These results highlight how polymer concentration, nanofiller content, and phase inversion dynamics collectively govern membrane porosity and structure.

Performance evaluations of nanocomposite membranes

Water permeation flux analysis

The water permeation flux in Fig. 6 showed a trend ranging from 124.09 to 1019.89 L/m^2·h, whereby the lowest water permeation flux recorded was S0 and the highest is S5. The S0 represents a pristine membrane, and S5 represents a nanocomposite membrane with 0.27 wt% NC and 10.72 wt% GO. The trends from the figure indicate that the incorporation of NC and GO has produced a significant impact on the permeation flux performance of the membranes, which also represents the membranes' permeability. However, a downward trend can be seen on S6 due to the absence of NC.

Pristine PVDF (S0) exhibited the lowest water flux, which can be attributed to its inherent hydrophobicity and relatively lower porosity, as shown in Fig. 5. As confirmed in the FTIR analysis, the presence of C-F stretching vibrations indicates the

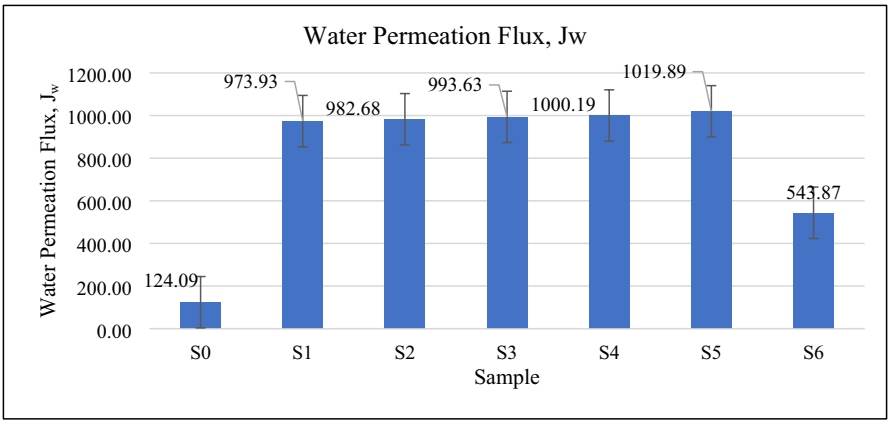

Fig. 6 Water permeation flux analysis of each membrane sample

fluorinated structure of PVDF, and these nonpolar fluorinated chains tend to resist water penetration, thus restricting water flow across the membrane. This can further be proven from the SEM analysis, whereby S0 has the least pore formations on its surface, which may have made it harder for the water molecules to pass through the membrane, resulting in low flux.

When 1.48 wt% NC was incorporated in S1, the water flux significantly increased to 973.93 L/m²·h. This improvement is due to the enhanced hydrophilicity and increased surface roughness introduced by NC. From the SEM image, an increase in pore formation can be seen, which provides a rough texture on its surface. This also leads to an increase in its porosity, which was proven from the membrane porosity result in Fig. 5. As mentioned before, higher porosity of the membrane leads to higher permeate flux [1]. The incorporation of NC had improved the hydrophilicity properties of the membrane, which may have led to the formation of more porous or interconnected structures during the phase inversion process, further facilitating water flow.

Samples S2 through S4, with varying ratios of NC and GO, demonstrated relatively stable and high fluxes, ranging from 982.68 to 1000.19 L/m²·h. The consistency of flux values in this range indicates that both fillers played complementary roles in improving the membrane's permeability. This may be attributed to the increase in GO concentration, leading to more presence of numerous oxygenated functional groups such as carboxyl and hydroxyl, which enhance the membrane's water affinity and facilitate solvent-nonsolvent exchange during membrane formation, promoting pore formation.

Among all samples, S5 exhibited the highest flux of 1019.89 L/m^2·h. This is due to its relatively high porosity (48.05%), which allowed more water particles to flow through the membrane. As shown in the FTIR result, the addition of NC and GO contributed to the presence of O-H functional groups that provide significant improvement in the hydrophilicity of the membrane. [2] stated that the integration of nanomaterials may cause polymer chains to dislocate, resulting in an increase in free volume or the formation of voids. The free volumes and more void formation

allowed water molecules to flow more freely through the membrane, thus increasing the permeation flux. The presence of hydrophilic additives is supposed to lead to increased permeability, which results in increased water permeation flux, shown in S5. This is due to the synergistic effect between PVDF, NC, and GO that improves its hydrophilicity properties, improving the water permeation flux and antifouling performance [16].

The decline of S6 with the permeation flux at 543.87 $L/m^2 \cdot h$ indicates that the absence of NC had affected the permeation flux result of the membrane. In the FTIR result, the addition of GO still showcased the presence of O-H functional groups, which still contributed to the hydrophilicity and permeability of the membrane even though NC was absent. S6 has the highest porosity compared to all of the samples, but the few pores that were formed on the surface, as shown in the SEM image, may have affected the amount of water allowed to pass through the membrane, making the flux less. The excessive GO loading or aggregation may also have led to partial blockage or densification of the membrane surface, reducing water transport pathways. The high crystallinity shown in its XRD result in Fig. 4 may have also lowered the water flux for S6. This also indicates that a suitable concentration of NC added plays an important role in improving the permeability of the membranes.

Overall, the results suggest that membrane flux is positively influenced by the presence of hydrophilic nanomaterials, especially when an optimal combination of NC and GO is used. These modifications improve both the membrane's wettability and morphology, which are key factors in high water flux performance. This finding aligns with previous studies by [16] and [2] that reported an enhancement in the permeation properties of the membranes that were modified with hydrophilic nanofillers.

Dye removal analysis

The dye removal performance shown in Fig. 7 indicates a trend of decreasing dye removal efficiency as the composition of the membrane is modified, highlighting the influence of nanoparticle incorporation and membrane morphology on separation efficiency. The pristine PVDF membrane (S0) showed the highest MB dye rejection at 87.40%, likely due to its dense structure and limited porosity. As seen in the SEM imaging, S0 has the lowest pore formation and smooth surface, which contributes to the high MB dye removal rates. The dense structure primarily restricts the passage of MB molecules through size exclusion, while the low porosity limits the number of available pathways for dye permeation.

A slight decrease in MB dye removal was observed in S1 (85.60%), potentially due to the introduction of NC (1.48wt%), which marginally altered the membrane's pore structure. The porosity result also showed a high porosity (48.05%), and also good dispersion of pores that can be seen from the SEM imaging. This combination of increased pore connectivity and hydrophilicity enhances water transport but slightly reduces the efficiency of size-based rejection. Additionally, hydroxyl groups on NC contribute to the adsorption of MB molecules via hydrogen bonding and electrostatic interactions, partially compensating for the larger pore size.

S2 through S4 demonstrated a gradual decrease in dye removal efficiency, ranging from 84.50% to 75.00%. These membranes contain varying compositions of NC

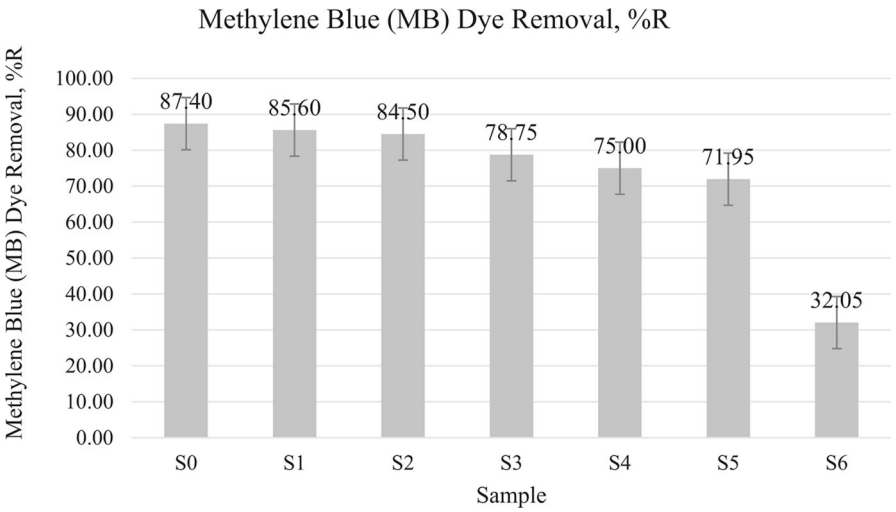

Fig. 7 Dye removal analysis of each membrane sample

and GO. While the addition of GO increases hydrophilicity and facilitates water flux, excessive GO can lead to structural defects or agglomeration, creating microchannels that allow MB molecules to permeate more easily. The negative surface charge of GO may reduce electrostatic attraction to the positively charged MB dye, thereby decreasing adsorption capacity.

S5 showed a noticeable decrease in dye removal performance to 71.95% despite having the highest water flux. In this case, the highly porous structure and enhanced hydrophilicity improve water transport but reduce the efficiency of molecular sieving. FTIR analysis shows a strong presence of hydroxyl groups (-OH) at 3313.71 cm-1, enabling π–π and hydrogen bonding interactions with MB molecules. XRD analysis indicates a slightly lower crystallinity, increasing amorphous regions that favor water permeability while maintaining some molecular sieving capability. Thus, the dye rejection mechanism in S5 involves a combination of size exclusion, electrostatic interaction, and hydrogen bonding/π–π interactions.

Out of all of the membranes, S6 has the lowest MB dye rejection rate, which is only up to 32.05%. Although S6 exhibits high porosity (48.54%), the absence of NC reduces structural stability, and the presence of cracks facilitates unimpeded passage of MB molecules. GO alone provides limited adsorption sites, and without NC, the membrane loses both mechanical support and effective dye–membrane interactions.

Overall, the dye rejection mechanism in these PVDF/NC/GO membranes is governed by a combination of (i) size exclusion due to pore dimensions and polymer matrix density, (ii) electrostatic interactions between membrane functional groups and charged dye molecules, (iii) hydrogen bonding and π–π interactions with nanofillers, and (iv) structural integrity provided by NC to maintain selective pathways. These findings highlight the importance of optimizing nanomaterial loading to achieve an ideal balance between water permeability and dye selectivity for effective wastewater treatment.

Conclusion

This study successfully developed and analyzed PVDF-based composite membranes incorporated with NC and GO using the NIPS method for dye removal in wastewater treatment. The results demonstrated that the incorporation of NC and GO significantly improved the physicochemical properties of the PVDF membranes. These enhancements were evident in the increased porosity, improved surface morphology, and greater hydrophilicity, which collectively contributed to better water permeation flux and dye rejection capabilities. Among all membrane samples, S5 exhibited the highest water flux, indicating excellent permeability compared to the unmodified/pristine PVDF membrane (S0). This enhancement is attributed to the hydrophilic functional groups introduced by NC and GO, which facilitate greater water passage. Additionally, the dye rejection performance was notably high in membranes with optimized NC and GO loading (10.72 wt% and 0.27 wt%, respectively), demonstrating effective contaminant removal. This can be linked to better interaction between the membrane surface and dye molecules as they pass through the membrane. XRD analysis revealed a trend of increased crystallinity, especially in sample S6. The higher crystallinity suggests improved membrane structural integrity, which is crucial for long-term operational stability. Overall, the PVDF/GO/NC composite membranes developed in this research exhibit promising insight for wastewater treatment applications, offering advantages in terms of filtration efficiency, pollutant removal, and membrane durability. Several recommendations are proposed to improve the performance and applicability of the developed membranes. Firstly, future studies should aim to optimize the concentrations of NC and GO to avoid agglomeration and ensure uniform dispersion, as excessive filler loading may negatively impact membrane structure, as stated by the previous studies. Next, long-term fouling resistance and operational stability should be assessed under real wastewater conditions to determine the membranes' practical durability, which also helps in predicting the operational costings. Finally, the scope of application should be expanded by evaluating the membranes' effectiveness in removing other pollutants such as heavy metals, pharmaceuticals, or microorganisms.

Acknowledgements The authors wish to acknowledge the financial support from the Universiti Malaysia Sarawak under VC High Impact Research Grant UNI/F07/VC-HIRG/85518/P12-03/2022. This research is also funded by Princess Nourah bint Abdulrahman University Researchers Supporting Project number (PNURSP2025R80), Princess Nourah bint Abdulrahman University, Riyadh, Saudi Arabia. Authors also acknowledge to University of Malaya BKP grant number: UM.0001172/HGA.GV.

Author contributions M. R. Rahman, N. F. Dollah Chek, M. K. B. Bakri: writing and editing original draft, validation, reviewing and editing the manuscript; M. S. Ahmmad, M. S. M. Al-Saleem, J Y. Al-Humaidi, M M. Rahman: reviewing and minor editing.

Funding Open access funding provided by The Ministry of Higher Education Malaysia and Universiti Malaysia Sarawak

Data availability All data used to prepare the manuscript are included. Additional explanation is available upon request.

Declarations

Conflict of interest The authors declare no competing interests.

Consent to participate All authors contributed to the study's conception and design. All authors read and approved the final manuscript.

References

1. Abdel-Karim A, Luque-Alled JM, Leaper S, Alberto M, Fan X, Vijayaraghavan A, Gorgojo P (2019) PVDF membranes containing reduced graphene oxide: effect of degree of reduction on membrane distillation performance. Desalination 452:196–207
2. Ahmad H, Zahid M, Rehan ZA, Rashid A, Akram S, Aljohani MM, Al-Harbi MS (2022) Preparation of polyvinylidene fluoride nano-filtration membranes modified with functionalized graphene oxide for textile dye removal. Membranes 12(2):224
3. Al-Tohamy R, Ali SS, Li F, Okasha KM, Mahmoud YAG, Elsamahy T, Mahmoud YA, Jiao H, Fu Y, Sun J (2022) A critical review on the treatment of dye-containing wastewater: ecotoxicological and health concerns of textile dyes and possible remediation approaches for environmental safety. Ecotoxicol Environ Saf 231:113160
4. An YC, Gao XX, Jiang WL, Han JL, Ye Y, Chen TM, Ren RY, Zhang JH, Liang B, Li ZL, Wang AJ, Ren NQ (2023) A critical review on graphene oxide membrane for industrial wastewater treatment. Environ Res 223:115409
5. Bhadra M, Roy S, Mitra S (2016) Desalination across a graphene oxide membrane via direct contact membrane distillation. Desalination 378:37–43
6. Cai X, Lei T, Sun D, Lin L (2017) A critical analysis of the α, β and γ phases in poly (vinylidene fluoride) using FTIR. RSC Adv 7(25):15382–15389
7. Du X, Shi Y, Jegatheesan V, Haq IU (2020) A review on the mechanism, impacts and control methods of membrane fouling in MBR system. Membranes 10(2):24
8. Fahma F, Febiyanti I, Lisdayana N, Arnata IW, Sartika D (2021) Nanocellulose as a new sustainable material for various applications: A review. Archives Mater Sci Eng 109(2)
9. Hassaan MA, Nemr E, A., Hassaan A (2017) Health and environmental impacts of dyes: mini review. Am J Environ Sci Eng 1(3):64–67
10. Hurwitz G, Guillen GR, Hoek EMV (2010) Probing polyamide membrane surface charge, zeta potential, wettability, and hydrophilicity with contact angle measurements. J Membr Sci 349(1–2):349–357. https://doi.org/10.1016/j.memsci.2009.11.063
11. Maggay IVB, Aini HN, Lagman MMG, Tang SH, Aquino RR, Chang Y, Venault A (2022) A bio-fouling resistant zwitterionic polysulfone membrane prepared by a dual-bath procedure. Membranes 12(1):69
12. Marshall JE, Zhenova A, Roberts S, Petchey T, Zhu P, Dancer CE, Goodship V (2021) On the solubility and stability of polyvinylidene fluoride. Polymers 13(9):1354
13. Namakka M, Rahman MR, Said K. A. M. Bin, Abdul Mannan M, Patwary AM (2023) A review of nanoparticle synthesis methods, classifications, applications, and characterization. Environmental Nanotechnology, Monitoring and Management 20(November):100900. https://doi.org/10.1016/j.enmm.2023.100900

14. Nguyen VT, Ha LQ, Nguyen TD, Ly PH, Nguyen DM, Hoang D (2021) Nanocellulose and graphene oxide aerogels for adsorption and removal methylene blue from an aqueous environment. ACS Omega 7(1):1003–1013
15. Otitoju TA, Ahmad AL, Ooi BS (2016) Polyvinylidene fluoride (PVDF) membrane for oil rejection from oily wastewater: a performance review. J Water Process Eng 14:41–59
16. Rahman MR, James A, Said KAM, Namakka M, Khandaker MU, Jiunn WH, Rahman MM (2024) A TiO 2 grafted bamboo derivative nanocellulose polyvinylidene fluoride (PVDF) nanocomposite membrane for wastewater treatment by a photocatalytic process. Mater Adv 5(19):7617–7636
17. Sahu D, Sarkar N, Sahoo G, Mohapatra P, Swain SK (2015) Silver imprinted graphene nanocomposites: synthesisis and morphological study. Appl Sci Adv Mater Int 1(6):224–227
18. Sakib AAM, Masum SM, Hoinkis J, Islam R, Molla MAI (2019) Synthesis of CuO/ZnO nanocomposites and their application in photodegradation of toxic textile dye. J Compos Sci 3(3):91
19. Salim N, Siddiqa A, Shahida S, Qaisar S (2019) PVDF based nanocomposite membranes: application towards wastewater treatment. Madridge J Nanotechnol Nanosci 4(1):139–147
20. Slama HB, Chenari Bouket A, Pourhassan Z, Alenezi FN, Silini A, Cherif-Silini H, Oszako Tomasz, Luptakova Lenka, Golińska Patrycja, Belbahri L (2021) Diversity of synthetic dyes from textile industries, discharge impacts and treatment methods. Appl Sci 11(14):6255
21. Tan HF, Tan WL, Hamzah N, Ng MHK, Ooi BS, Leo CP (2020) Membrane distillation crystallization using PVDF membrane incorporated with TiO2 nanoparticles and nanocellulose. Water Supply 20(5):1629–1642
22. United Nations Environment Programme (2023) Wastewater – Turning problem to solution: A UNEP rapid response assessment. United Nations Environment Programme, Nairobi, Kenya. https://doi.org/10.59117/20.500.11822/43142
23. United Nations Educational, Scientific and Cultural Organization (2015) UNESCO project on emerging pollutants in wastewater reuse in developing countries. Paris. https://unesdoc.unesco.org/ark:/48223/pf0000235241
24. Wu Q, Chen Q (2020) Application of membrane separation technology in water treatment process. IOP Conf Series: Earth Environ Sci 508:012048. https://doi.org/10.1088/1755-1315/508/1/012048
25. Zhao Q, Yang H, Tong L, Jin R (2023) Pollution characteristics of pyrite surface in cyanide tailings by PCA-assisted ToF-SIMS and their correlation with the contact angle. JOM 76(1):547–557. https://doi.org/10.1007/s11837-023-06143-4

Authors and Affiliations

Md. Rezaur Rahman[1] · Nur Fatmadewi Dollah Chek[1] · Muhammad Khusairy Bin Bakri[1,2] · M. Shahabuddin Ahmmad[3] · Muneera S. M. Al-Saleem[4] · Jehan Y. Al-Humaidi[4] · Mohammed M. Rahman[5]

✉ Md. Rezaur Rahman
rmrezaur@unimas.my

✉ Muhammad Khusairy Bin Bakri
kucaigila@yahoo.com

[1] Faculty of Engineering, Universiti Malaysia Sarawak, Jalan Datuk Mohammad Musa, 94300 Kota Samarahan, Sarawak, Malaysia

[2] Composite Materials and Engineering Center, Washington State University, 2001 East Grimes Way, 99164 Pullman, Washington State, USA

[3] Department of Mechanical Engineering, Faculty of Engineering, University of Malaya, 50603 Kuala Lumpur, Malaysia

[4] Department of Chemistry, Science College, Princess Nourah bint Abdulrahman University, P.O. Box 84428, Riyadh 11671, Saudi Arabia

[5] Center of Excellence for Advanced Materials Research (CEAMR) & Chemistry Department, Faculty of Science, King Abdulaziz University, Jeddah 21589, Saudi Arabia